Comput Geosci (2008) 12:15–27
DOI 10.1007/s10596-007-9058-6

ORIGINAL PAPER

Mortar coupling and upscaling of pore-scale models

Matthew T. Balhoff · Sunil G. Thomas · Mary F. Wheeler

Received: 19 January 2007 / Accepted: 19 August 2007 / Published online: 27 September 2007

Abstract Pore-scale models are becoming increasingly useful as predictive tools for modeling flow and transport in porous media. These models can accurately represent the 3D pore-structure of real media. Currently first-principles modeling methods are being employed for obtaining qualitative and quantitative behavior. Generally, artificial, simple boundary conditions are imposed on a model that is used as a stand-alone tool for extracting macroscopic parameters. However, realistic boundary conditions, reflecting flow and transport in surrounding media, may be necessary for behavior that occurs over larger length scales or including pore-scale models in a multiscale setting. Here, pore-scale network models are coupled to adjacent media (additional pore-scale or continuum-scale models) using mortars. Mortars are 2D finite-element spaces employed to couple independent subdomains by enforcing continuity of pressure and flux at shared boundary interfaces. While mortars have been used in the past to couple subdomains of different models, physics, and meshes, they are extended here for the first time to pore-scale models. The approach is demonstrated by modeling single-phase flow in coupled pore-scale models, but the methodology can be utilized to model dynamic processes and perform multiscale modeling in 3D continuum simulators for flow and transport.

Keywords Pore-scale modeling · Network modeling · Multiscale modeling · Mortar coupling · Upscaling

M. T. Balhoff (✉) · S. G. Thomas · M. F. Wheeler
Texas Institute for Computational and Applied Mathematics, University of Texas, Austin, TX 78712, USA
e-mail: balhoff@mail.utexas.edu

1 Introduction

Flow and transport in porous media is typically modeled at the continuum scale by solving the continuity equation together with momentum, energy, and/or species balances. Constitutive equations, such as Darcy's law, are substituted into these equations for velocity. Quantitative values of empirical parameters, such as permeability, relative permeability, and capillary pressure, are needed as inputs for the model, which are dependent on the media morphology and/or the fluids in the pore space. Experimental measurements are commonly used to estimate the parameters used for direct substitution into continuum simulators, but recently, pore-scale models have become a popular and efficient method for parameter estimation.

Network modeling is a pore-scale technique in which the porous medium is approximated as an interconnected network of pores and pore throats. Network models have long been used to study important behavior regarding flow and transport in porous media but were limited to qualitative studies because simple 2D or 3D lattices were used. More recently, quantitative techniques have been developed to model certain behavior in porous media including single-phase Newtonian flow [10], multiphase flow [8], and non-Newtonian flow [5, 18]. Physically representative network models [10] are mapped directly from a rigorous description of some original well-described porous medium, and consequently, they retain important morphology and spatial correlations that are necessary for obtaining quantitative and predictive results. To make network modeling as predictive as possible, advancements continue to be made in two specific areas: (1) characterization of the 3D pore structure and transformation into a physically representative network model and (2) accurate

flow modeling in the resulting network using a first-principles approach.

The first step in characterizing the pore structure is to obtain an accurate, numerical description of the porous medium. X-ray computed microtomography (XMT) [15, 17, 26] is a technique used to extract the 3D pore structure of real, naturally occurring porous media. The high-resolution images obtained through XMT are digitally represented as voxels, which (in a binary image) define the pore and grain space. Computer-generated methods offer an alternative to high-resolution imaging of porous media. These methods include stochastic approaches [1, 15] in which the porous medium is reconstructed using statistical properties and process-based approaches that attempt to simulate the geological process in which the medium is formed. For example, Baake and Oren [8] have created computer-generated sandstones by modeling sedimentation, compaction, and diagenesis. Regardless of the method used to digitally represent the medium, the second step is conversion to a network model of pores and throats. Grain-based methods are usually tied to approaches that represent grain positions in porous media. Bryant et al. [10] used a Delaunay tessellation to determine the pores and interconnected throats to create a physically representative network model. Al-Raoush et al. [2] extended that work by using a modified Delaunay tessellation, which allowed the pore interconnectivity to vary. For voxel data obtained from imaging, the medial-axis [16, 22] can be used to thin the void space, from which one can map out the pores and throats in the network. Recently, a grain-based reconstruction algorithm [23] was created to generate network models from voxel data. Advantages of this method include its insensitivity to image resolution and the mapping of the network from fundamental building blocks in the material (i.e., the grains).

Once the network model is generated, it can be used to model a wide range of flow and transport problems by forcing mass conservation at every pore and solving fundamental equations of momentum, mass, and heat transfer in the connecting throats. Early network modeling assumed throats were simple capillary tubes or transformed the throats into equivalent capillaries [10, 18] so that the Navier–Stokes equations, etc., could be solved in a straightforward manner. Advancements continue to be made to account for the actual irregular geometry of these throats. Balhoff and Thompson [5, 6] have developed closed-form empirical flow equations for non-Newtonian fluids in converging/diverging ducts (which are more representative of the true throat geometry) by solving the momentum equations numerically.

The recent improvements in these two areas (characterization of the pore structure and flow modeling) has allowed network modeling to become more of a predictive tool for obtaining upscaled, macroscopic parameters. Despite these advancements, simple boundary conditions (usually a pressure gradient in one dimension) are almost always imposed when flow modeling is performed. Because the pore-scale model often represents a portion of a much larger medium, the true boundary conditions should depend on flow behavior in the surrounding media. Imposing artificial boundary conditions can lead to misleading upscaled values, whereas choosing appropriate boundary conditions on the network require direct coupling to adjacent media (additional pore-scale or continuum-scale models). The later procedure is not straightforward because the models are independent and the boundary pores may not be naturally connected to the adjacent model.

Recently, Balhoff et al. [7] developed a domain-decomposition method for coupling a pore-scale model to an adjacent continuum model. In that approach, a pressure field is determined iteratively at the interface such that flow in/out of every boundary pore of the network model matches the total flow out/in of the continuum region (integrated over an area corresponding to each specific pore). The resulting interface boundary conditions were very complex due to the heterogeneity captured in the pore-scale models. It was shown that the boundary conditions could be significantly different for two similar realizations (with identical macroscopic properties such as grain diameter, porosity, and permeability) because the pore structure is different. Implementing a simple boundary condition (such as a constant pressure, linear pressure profile, or one obtained by approximating the pore-scale region as a continuum) was also shown to result in incorrect qualitative and quantitative results. While this multiscale approach provides a motivation for determining realistic boundary conditions by coupling to adjacent media, it has limited practicality. First, the continuum model in that work was simple and amenable to an analytical solution, so fluxes could be evaluated easily at the discrete point corresponding to the boundary pore positions in the adjacent network model. The method would not be applicable for coupling two discrete network models because the boundary pore positions would not match in general. Second, the approach can be very computationally inefficient because it involves solving M simultaneous equations (M being the number of boundary pores). Each subdomain must be solved M times to generate the Jacobian for the interface problem, and it becomes obvious that this is not computationally efficient, especially for nonlinear and time-dependent problems.

A domain decomposition approach using mortars has been developed [3] to model flow and transport in porous media. This has been implemented in the research software

Integrated Parallel Accurate Reservoir Simulator. The decomposed subdomains can model different physics, contain different models, or implement different finite-difference or finite-element meshes [3, 4, 12, 20, 25, Girault et al. 2007, in review]. The subdomains are solved independently and the interface boundary conditions are determined using mortar spaces. The mortar space is a 2D, finite-element space that is used to project primary variables (e.g., pressure) onto the subdomain. The projected pressure field must be chosen so that the jump in secondary variables (e.g., fluxes) is zero, thus maintaining continuity. Accuracy can be improved by utilizing finer meshes on the mortar space or using higher-order mortars such as linear or quadratic basis functions [see 4]. Because the subdomains in the mortar method are solved independently, they can be viewed as "black boxes" and thus could be models at different scales. However, the mortar coupling method has not yet been extended to include pore-scale models. The method would have some advantages over the method used by Balhoff et al. [7] for that application in that each element would contain several pores, and therefore, a significantly fewer number of interface equations would have to be solved. Zhodi and Wriggers [27] did use a novel domain decomposition approach to couple microscale models, but the interface boundary conditions were not chosen rigorously. They modeled mechanics at a continuum scale and then used the solution to impose boundary conditions at the subdomain interfaces. Balhoff et al. [7] showed some of the limitations of utilizing boundary conditions in this manner.

A number of other methods have been developed to perform multiscale modeling in solid mechanics by coupling atomistic and continuum approaches. Kohloff et al. [14] modeled mechanics in an atomistic domain surrounded by a continuum, finite-element mesh. Boundary conditions at the interface were determined by ensuring consistency in strains in a small overlap region. Broughton et al. [9] extended the work of Kohloff et al. using molecular-atomistic-ab initio dynamics by refining the continuum, finite-element mesh to the atomic scale in the overlap region. Wagner and Liu [24] have developed a bridging scale technique in which the atomistic and continuum scales completely overlap. More information on these multiscale methods can be found in the review by Rudd and Broughton [21], as well as in an introduction by Klein and Zimmerman [13].

The objective of the current work is to model flow in porous media by coupling pore-scale network models to other pore-scale or continuum-scale models using mortars at the interface. The mortars provide a method for determining realistic boundary conditions on predictive pore-scale models because they are intended to represent a portion of a much larger porous medium. The outline of the paper is organized as follows: In Section 2 the mathematical approach for network modeling is discussed. The equations for mortar coupling these pore-scale models to other pore-scale or continuum-scale models are then presented. In Section 3 the coupling method is verified by coupling two identical, periodic pore-scale models and comparing this unique case to the actual interface pressure field. In Section 4, different pore-scale models are coupled together; both qualitative and quantitative results are discussed. Additionally, a pore-scale model is coupled to surrounding continuum-scale models. Finally, in Section 5, conclusions and future applications of the work are discussed.

2 Mathematical approach

2.1 Network modeling

Although pore-scale models have been used in the past as qualitative tools for modeling flow and transport in porous media, today, physically representative [10] models of heterogeneous 3D structures can be used to obtain predictive information for upscaling. The first step in network modeling is to obtain a 3D representation of the porous medium. These structures can be computer-generated sphere packings [2], computer-generated synthetic sandstones, or X-ray computed tomography of real reservoir sandstones or consolidated rock. For example, Fig. 1a is a sample sandstone structure from the Frontier Formation in Wyoming, USA [11], and Fig. 1b is the network model mapped from the sandstone [23]. In this work, both computer-generated sphere packings and sample sandstones imaged using XMT will be used as representative porous media. Sphere packings can represent certain unconsolidated media in subsurface applications, such as proppant

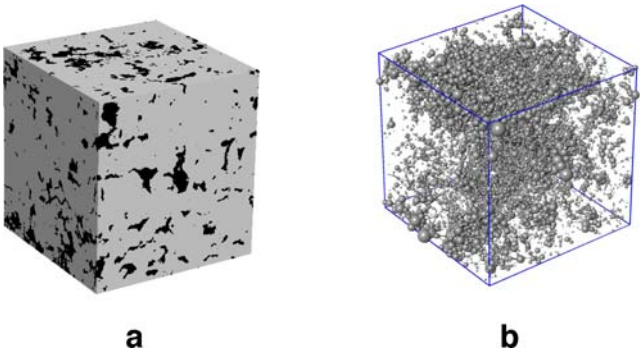

Fig. 1 **a** Sample sandstone structure from the Frontier Formation in Wyoming, USA [11] and **b** the resulting pore-scale network model [23]

particles in propped hydraulic fractures or weathered, unconsolidated sands. These structures can be created quickly with specified porosity, grain-size distribution, and spatial correlation.

In each of the media described above, specification of the position and size of each grain is sufficient to completely define the structure of the void space in which fluid is transported. However, it is a continuous, interconnected region with a complex geometry, and hence, some form of discretization is required prior to numerical simulation. In the network-modeling approach, the continuum void space is discretized into pores and pore throats. The challenge is to obtain a network structure that effectively represents the true pore-space morphology.

Here, networks were generated using a modified Delaunay tessellation algorithm [2]. In the network generation process, several rigorous geometric parameters are used to describe the network, along with the hydraulic conductivity of each throat in the network, which is computed based on the local pore and pore-throat geometry.

The general approach to network modeling is to impose a mass conservation equation at each pore in the network. For constant-density fluids, the conservation equation for pore i is simply

$$\sum_j q_{ij} = 0 \tag{1}$$

where q_{ij} is the volumetric flowrate into pore i through a throat connected to neighbor j. The flowrate q_{ij} is then written in terms of unknown pore pressures, which become the dependent variables in the problem. For low-Reynolds-number flow of Newtonian fluids, flowrate is linearly proportional to the pressure drop for all the pore-throat geometries.

2.2 Mortar coupling

Domain decomposition can be an efficient way to solve large problems because the decomposed subdomains may be solved in parallel. Additionally, the subdomains may be used to model different physics, meshes, or scales. This allows for focusing the computational effort where it is needed. A disadvantage of domain decomposition is that boundary conditions must be imposed on the subdomains and, if chosen incorrectly, pressures and fluxes would not match at the interface. Mortars are a way of coupling decomposed subdomains by enforcing continuity of pressures and fluxes at their shared boundaries. Mortar spaces are 2D finite-element spaces imposed at the interface of subdomains, and they are used as a tool for determining the shared boundary condition (pressure field) so that continuity in fluxes is maintained.

The mortar spaces are first discretized into finite-element meshes. Following Arbogast et al. [4], a pressure field on the mortar space is chosen using basis functions (constants, linears, quadratics, etc.) on the elements. The pressure field is projected onto the adjacent face of each subdomain, and the resulting boundary condition is used to solve the subdomain problem. The fluxes (obtained from solution to the subdomain problem) are forced to match weakly when projected back to the mortar. Determination of the pressure field (i.e., the coefficients of the basis functions) requires the solution of a system of interface equations.

Here, the concept of mortar spaces is extended to include discrete network models that are coupled to additional network models or continuum-scale models. For clarity, the mathematical formulation in Arbogast et al. [4], with the necessary changes as applicable to the pore-scale model, is presented. Let $\Omega = \bigcup_{i=1}^{n} \Omega_i^{s_i}$ be a domain decomposed into n nonoverlapping subdomain blocks, $\Omega_i^{s_i}$, with $\Omega^s = \bigcup_i \Omega_i^{s_i}$, where s_i=p or c, depending on whether the subdomain is a pore-scale network or a continuum scale, respectively.

Further, let $\Gamma_{ij} = \partial\Omega_i^{s_i} \cap \partial\Omega_j^{s_j}$ denote the interface between the ith and jth subdomains. Next, let $\Gamma = \cup_{i,j=1}^{n} \Gamma_{ij}$ be the union of all such interfaces and, finally, denote the interfaces associated with the ith domain by $\Gamma_i = \partial\Omega_i^{s_i} \cap \Gamma = \partial\Omega_i^{s_i} \backslash \partial\Omega$. Here, we also define $\mathbf{V}_i = H\left(\mathrm{div}; \Omega_i^c\right) = \left\{\mathbf{v} \in \left(L^2\left(\Omega_i^c\right)\right)^d : \nabla \cdot \mathbf{v} \in L^2\left(\Omega_i^c\right), \mathbf{v} \cdot \mathbf{n} = 0 \text{ on } \partial\Omega_N \cap \partial\Omega_i^c\right\}$, where d is the dimension of the problem space and $\partial\Omega_N$ represents the part of the external domain with prescribed no-flow boundary conditions. The solution for velocity in the continuum subdomains belong to the spaces $\mathbf{V}_i$. Next, let $\mathbf{V} = \bigoplus_{i=1}^{N_c} \mathbf{V}_i$ be the "direct sum" of the spaces $\mathbf{V}_i$. Similary, for pressure in the ith continuum subdomain, define $W_i = L^2\left(\Omega_i^c\right)$ to be the solution space and let $W = \bigoplus_{i=1}^{N_c} W_i$ be the direct sum. Here, N_s is used to indicate the total number of "s-scale" subdomains.

It is also important to define the grids used in the continuum subdomains for an analysis of approximate solutions to the finite-element problem. Let $\mathrm{T}_{h,i}^c$ be a finite-element partition of the continuum subdomain, Ω_i^c, where h represents the maximal element diameter in the partition. Next, let $\mathrm{T}_{h,ij}^M$ be a similar (coarser) finite-element partition of the mortar interface Γ_{ij} and let $\mathrm{T}_h^M = \bigcup_{i,j} \mathrm{T}_{h,ij}^M$. Then, for finite-element approximations to the velocity and pressure, let $\mathbf{V}_{h,i} \times W_{h,i} \subset \mathbf{V}_i \times W_i$ be any of the usual mixed finite-element spaces (e.g., the RTN_0 space [19]) on the continuum subdomains. For pressures on the interface, define the space $M_h(\Gamma) \subset L^2(\Gamma)$ to be a mortar finite-element approximation space on the mortar interface, Γ; for example, the space of piecewise constants, continuous/discontinuous piecewise linears, or quadratics.

Then, $\mathbf{V}_h = \bigoplus_{i=1}^{N_c} \mathbf{V}_{h,i}$ and $W_h = \bigoplus_{i=1}^{N_c} W_{h,i}$ form the finite-element approximation spaces for the solution on the

continuum subdomains. To present completely the equations for the steady-state (and incompressible) problem under consideration, suppose that f is a source term in the continuum domains. Note that f is identically zero in all the numerical experiments presented because the flow is driven by the boundary conditions. Let g represent the function that prescribes the pressure on the Dirichlet portion of the external boundary, $\partial\Omega_D$. Then, introducing $\mathbf{u} = -\mathbf{K}\nabla p$ to denote the Darcy velocity in Ω^C, we seek, using a mixed finite-element approximation space in the continuum subdomains and a discrete space in the pore-scale subdomains:

$$\mathbf{u}^c_{h,i} \in \mathbf{V}_{h,i}\left(\Omega^c_i\right) \subset \mathbf{V}, p^c_{h,i} \in W_{h,i}\left(\Omega^c_i\right) \subset W, \left\{p^p\left(\mathbf{x}_{i,k}\right) : \mathbf{x}_{i,k} \in \Omega^p_k\right\} \in \Re^{N_{\Omega^p_k}} \text{ and } \lambda_h \in M_h(\Gamma)$$

such that, for $1 \le i \le N_c$,

$$\begin{aligned} \left(\nabla \cdot \mathbf{u}^c_{h,i}, w\right)_{\Omega^c_i} &= (f, w)_{\Omega^c_i}, && \forall w \in W_{h,i} \\ \left(\mathbf{K}^{-1}\mathbf{u}^c_{h,i}, \mathbf{v}\right)_{\Omega^c_i} &= \left(p^c_{h,i}, \nabla \cdot \mathbf{v}\right)_{\Omega^c_i} - <\lambda_h, \mathbf{v}\cdot\mathbf{n}_i>_{\Gamma_i} - <g, \mathbf{v}\cdot\mathbf{n}_i>_{\partial\Omega^c_i \cap \partial\Omega_D} && \forall \mathbf{v} \in \mathbf{V}_{h,i} \end{aligned} \tag{2}$$

and for $1 \le k \le N_p$,

$$\begin{aligned} &\sum_{j=1}^{n_i} q^p_{ij,k} = 0, \quad 1 \le i \le N_{\Omega^p_k} \quad \text{where } n_i \text{ is the number of pores connected to pore } i \\ &q^p_{ij,k} = \gamma_{ij,k}\left(p^p_{i,k} - p^p_{j,k}\right) \quad \text{and b.c's given by,} \\ &p^p_{i,k} = \begin{cases} g(\mathbf{x}_i), & \mathbf{x}_i \in \partial\Omega^p_k \cap \partial\Omega_D \\ \Pi\lambda_h(\mathbf{x}_i), & \mathbf{x}_i \in \partial\Omega^p_k \cap \Gamma \end{cases} \end{aligned} \tag{3}$$

with the interface condition:

$$\sum_{i=1}^{n} <\mathbf{u}^{s_i}_{h,i}\cdot\mathbf{n}_i, \mu>_{\Gamma_i} = 0 \qquad \forall \mu \in M_h(\Gamma), \tag{4}$$

where, in Eq. 3, $\mathbf{x}_i$ is the pore location, $\gamma_{ij,k}$ is the conductivity of the throat connecting pores i and j in the kth (pore-scale) subdomain, $q^p_{ij,k}$ represents the flux through these pores, and $N_{\Omega^p_k}$ denotes the total number of pores in that subdomain. In Eq. 4, $\mathbf{n}_i$ is the unit outward normal to Γ_i and $\mathbf{u}^{s_i}_{h,i}\cdot\mathbf{n}_i$ is the flux on the face Γ_i, which is clearly the usual flux for the continuum subdomains but is not so obvious for the noncontinuum case and needs definition. For a pore-scale subdomain (indexed i), it is computed by introducing a discretization $K(\Gamma_i)$ of the face Γ_i and defining the flux through an element e of the discretization as follows:

$$\mathbf{u}^p_{h,k}\cdot\mathbf{n}_k\Big|_e = \sum_{i,j} q^p_{ij,k} : \mathbf{x}_{i(j)} \in e, \forall e \in K(\Gamma_i). \tag{5}$$

Equation 5 essentially amounts to summing all the fluxes, $q^p_{ij,k}$ through pore-throats that cut across the element e. Equation 4 enforces weak continuity in the flux variable, which is now well-defined for both scales, across the subdomain interfaces. $\prod$ is a suitably defined L^2 projection operator that maps the pressure in the mortar space onto the subdomain face; for details, the reader may refer to Eq. 2.13 in Arbogast et al. [4]. The pressures are projected from the mortar space to the discretization $K(\Gamma_i)$ introduced on the pore-scale face adjacent to the mortar interface. Implicit in the interface boundary condition of Eq. 3 is an interpolation to the specific pore-location in question. It can be shown (see Arbogast et al. [4] for proof) that the system of Eqs. 2–4 can be reduced to an interface formulation in λ_h. This system is simpler to solve than the scheme described in Section 1 because the mesh on the mortar interface can be made as coarse as desirable. For the numerical results presented, we use a conjugate gradient method to solve the resulting interface equation. Proofs of convergence or existence/uniqueness are beyond the scope of the current work, but numerical results are presented to demonstrate their validity.

3 Model verification

Mortars provide an efficient method for coupling pore-scale models and determining approximate boundary conditions at interfaces. Here we attempt to demonstrate that the resulting boundary conditions are correct and also to determine the effect of mesh size and basis functions on

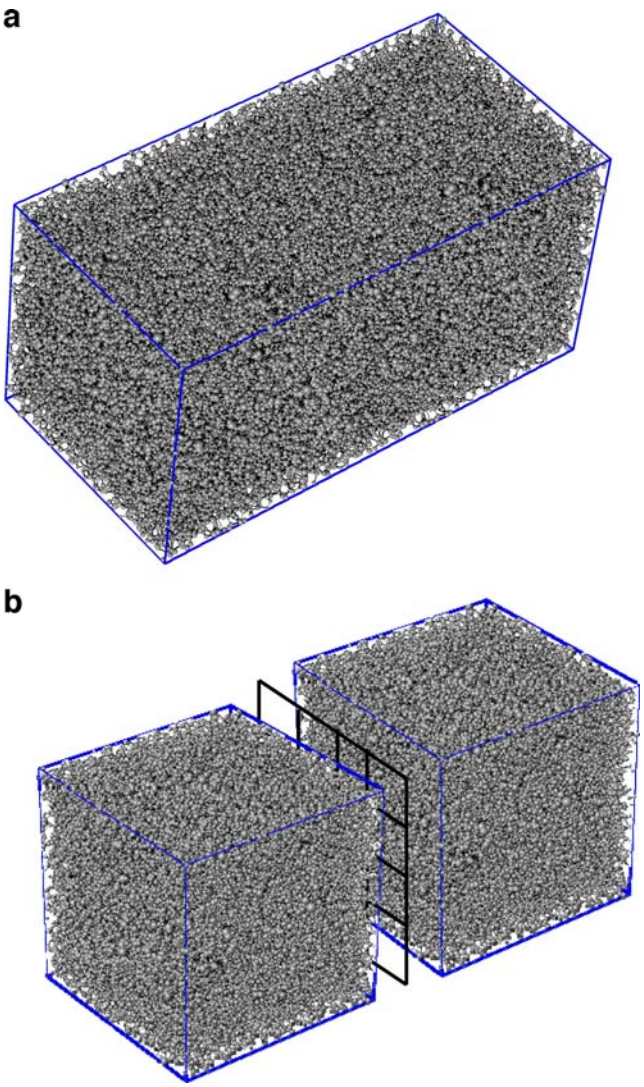

Fig. 2 **a** Network model obtained from a periodic, computer-generated sphere packing and then replicated to produce one large network and **b** the original network model coupled to its replica using a 4×4 mortar space

the accuracy. It is not possible in general to determine the actual interface boundary conditions for two or more coupled pore-scale models (motivation for mortar coupling) because the discrete networks are independent models and pores are not connected at the interface boundaries.

A model problem is created here to demonstrate the mortar approach for coupled pore-scale models; a periodic, computer-generated sphere packing is coupled to an exact replica of itself. The original medium has 10,000 uniform-sized spheres with a porosity of 38% and particle diameter of 0.049 cm. The resulting network has 41,273 interior pores, 826 and 847 boundary pores on their left and right faces, respectively (these two sets of boundary pores are adjacent at the interface when the network is coupled to its replica), and the network has a permeability of 2.4×10^{-6} cm^2.

Figure 2a is the fully coupled, single domain where the pore-scale models are naturally connected by throats through the periodicity; Fig. 2b shows the individual pore-scale models coupled via mortars. Simulations were performed for the realizations shown in Fig. 2a and b by enforcing a pressure gradient in one direction (a constant pressure was placed on each side of the domain, $P=0.3$ Pa and $P=0.1$ Pa) and flow was simulated as described in the previous section. Because the two domains in Fig. 2b are identical and therefore have the same macroscopic permeability, an interface pressure of exactly 0.2 Pa would seem reasonable. In fact, that boundary condition results in a total flowrate exiting subdomain 1 that matches the flowrate entering subdomain 2. However, closer inspection shows that interface boundary condition is not correct and the flowrates match poorly at a smaller scale as shown in Fig. 3.

Figure 4 is the contour plot of the actual pressure field at the interface for the fully coupled case (Fig. 2a). Pressures are only known at discrete points (the pore positions), and the pressure field in the figure is found using an interpolating function in MATLAB. The figure reflects the

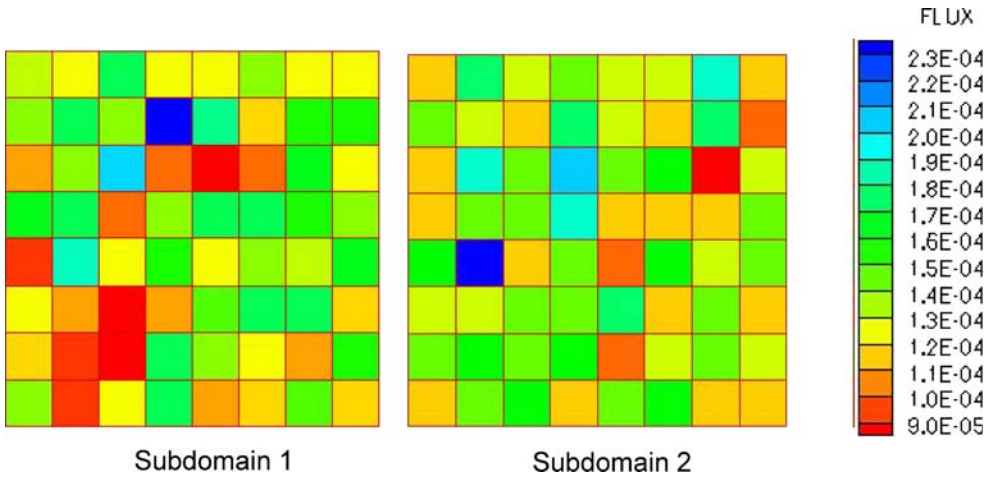

Fig. 3 Flux comparison at the interface for pore-scale models on an 8×8 grid for the uniform pressure, $P=0.2$ Pa

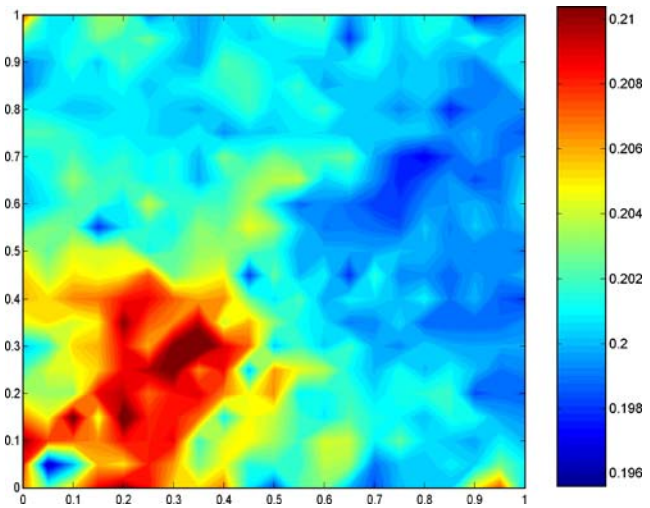

Fig. 4 Contour plot of pressure field at the centerline of the network model in Fig. 2a

heterogeneity captured by the pore structure. The pressure varies from approximately $P=0.195$ to $P=0.209$ at the interface, which is significant given the total pressure difference in the coupled domains. It is apparent that the pressure is significantly higher (on average) in the area of the lower-left quadrant. Higher pressures are required because of some relatively low conducting throats in that region. It is obvious that utilizing an average pressure of $P=0.2$ would not be able to correctly capture this behavior, and it is not surprising that the simple boundary condition results in the poor match in flowrates shown in Fig. 3.

The objective is to determine a pressure field using mortars that results in weakly matched fluxes at the interface. The resulting pressure field and fluxes should then approximate the true solution corresponding to Fig. 4 (it is important to note that this is a unique example in which we are able to find an "actual" solution). Pressure fields have been found using mortar coupling with various grids (2×2, 4×4, 8×8) and orders (constant, linear, and

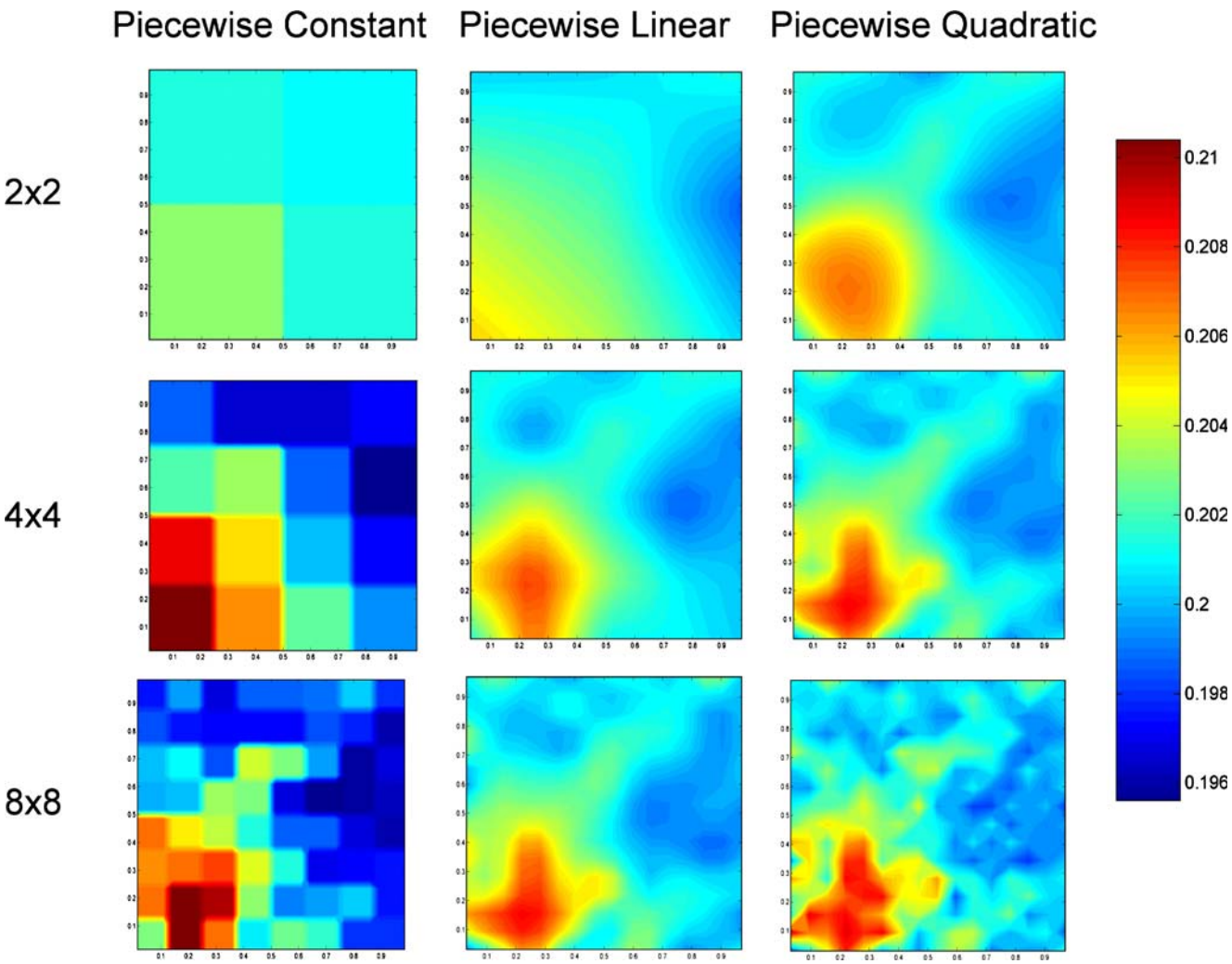

Fig. 5 Comparison of contour plots for the mortar space for the coupled networks in Fig. 2b using various meshes and basis functions

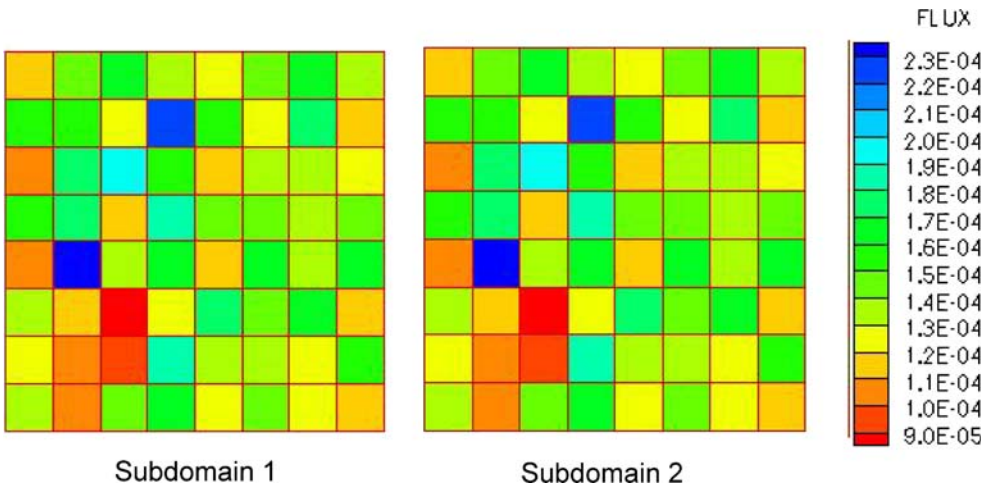

Fig. 6 Flux comparison at the interface for pore-scale models on an 8×8 grid the detailed pressure field obtained from mortar coupling using 8×8 mortar grid and quadratic basis functions

quadratic) and are shown in Fig. 5. The figures demonstrate that more detail is included for the finer mortar grids and higher-order mortars; they also appear to result in better qualitative matches to the actual pressure field in Fig. 4. Specifically, the mortars are able to reproduce the relatively high pressures in the lower-left quadrant. Figure 6 shows that the fluxes match at the interface for this pressure field much better than the results shown in Fig. 3.

Table 1 compares errors in fluxes across the interface for various mortar degrees of freedom and basis functions as described above. This error is measured by calculating the difference between the "actual" flux at the interface (which is obtained by projecting the flux on a sufficiently fine discretization of the midsection of the naturally coupled, single, pore-scale network onto the finest mortar space in each case, i.e., 8×8 constants, continuous linears, and continuous quadratics) and the corresponding flux obtained using the mortar finite-element approach. The resulting error is then normalized by the value of the actual flux at the interface. Thus, letting $\mathbf{u}$ represent the actual flux and $\mathbf{u_h}$ the approximate flux obtained in the coupled, mortar solution, we have

$$e(\mathbf{u_h}) = \frac{\left| \int_\Gamma (\mathbf{u} - \mathbf{u_h}) \cdot \mathbf{n} ds \right|}{\left| \int_\Gamma \mathbf{u} \cdot \mathbf{n} ds \right|}. \tag{6}$$

Table 1 Comparison of flux errors across the interface for various mortar spaces

	Constants	Linears	Quadratics
1×1	1.08×10^{-2}	1.03×10^{-2}	1.00×10^{-2}
2×2	1.03×10^{-2}	1.00×10^{-2}	9.69×10^{-3}
4×4	1.00×10^{-2}	9.69×10^{-3}	7.70×10^{-3}
8×8	9.12×10^{-3}	7.72×10^{-3}	3.29×10^{-3}

Because the interface formulation reduces to forcing weak continuity of fluxes as in Eq. 4, the error given by Eq. 6 is a measure of the convergence of the method.

The table demonstrates that higher-order mortars and finer grids result in a smaller error in flux when compared to the actual solution. Alternatively, one could define an error at the pore-level by comparing predicted and actual pore pressures (or flowrates) as is shown in Eq. 7 (although we note that the mortars are not intended to capture heterogeneity at this scale).

$$e(\mathbf{P}_{\text{discrete}}) = \frac{\sum_{i=1}^{M} \left| P_{i,\text{actual}} - P_{i,\text{predicted}} \right|}{M\ \Delta P} \tag{7}$$

The error in the equation is normalized by M and ΔP (the total applied pressure drop across the domain) so that the maximum possible error is 1.0. Table 2 clearly shows a general trend of improved accuracy with both finer grids and higher-order mortars. As a point of comparison, the simplest boundary condition, a 1×1 constant mortar corresponding to $P=0.2$ Pa, results in an error of 9.69×10^{-3}. The quantitative results in the table show that all of the mortar solutions result in a relatively low error in pore pressure, which is in agreement with the qualitative results in Figs. 3 and 4. However, the accuracy is problem-specific, as is the trade-off between accuracy and computational requirements.

The mortars are intended to approximate the boundary condition and give accurate results locally by averaging.

Table 2 Comparison of errors for various mortar spaces

	Constant	Linear	Quadratic
2×2	8.35×10^{-3}	7.02×10^{-3}	5.93×10^{-3}
4×4	7.38×10^{-3}	5.81×10^{-3}	5.51×10^{-3}
8×8	6.54×10^{-3}	5.51×10^{-3}	6.11×10^{-3}

The error at the pore-scale cannot be eliminated, and in fact, there is no guarantee that the error defined in Eq. 7 will be reduced by using finer mortar grids or higher-order basis functions (the 8×8 quadratic result is actually higher than some of the other errors) because the method is unable to capture large fluctuations in pressure at the pore scale. For example, consider two boundary pores at positions $x=0.269$, $y=0.294$ and $x=0.272$, $y=0.304$, which nearly coincide. For 4×4 quadratic mortars, the pore pressures are found to be $P=0.206$ and $P=0.207$, respectively, which are very close, as expected. However, the actual solution is $P=0.198$ and $P=0.210$, respectively, which is a large fluctuation for two adjacent pores. Regardless of the discretization, the mortar is not intended to capture heterogeneity at this scale.

Furthermore, it should be noted that extremely fine grids on the mortars can actually lead to less accuracy at the pore-scale for applications (such as the one here) where the subdomains are discrete and have a finite number of pores. In the extreme case, mortars can be chosen so fine that some elements contain no pores and the system of equations becomes singular. More generally, certain elements may contain a very small number of pores; attempting to match pressures and fluxes across that element may not be practical and can result in heterogeneity in the pressure solution that is not associated with the physics.

4 Results/discussion

4.1 Coupling different pore-scale models

Figure 7 shows four different pore-scale models coupled in a 2×2 block pattern. The statistics of the blocks are given in Table 3; block 1 is a computer-generated sphere packing with 1,000 uniform spheres; block 2 is a computer-generated sphere packing with 10,000 uniform spheres; block 3 is a sandstone with 2,487 grains taken from the Wall Creek Member of the Cretaceous Frontier Formation, WY, USA [11, 23]; and block 4 is a sphere-packing with 10,000 spheres with a size distribution and a spatial correlation. A 1D pressure gradient is imposed on the porous media by imposing a constant pressure on each boundary ($P=0.3$ and $P=0.1$ Pa) and no-flow boundaries on the other four boundaries. The exterior boundary conditions are obviously artificial; in reality, they would be determined from additional coupling to other models. The pore-scale models are coupled at each interface using mortar spaces with 4×4 grids and quadratic basis functions.

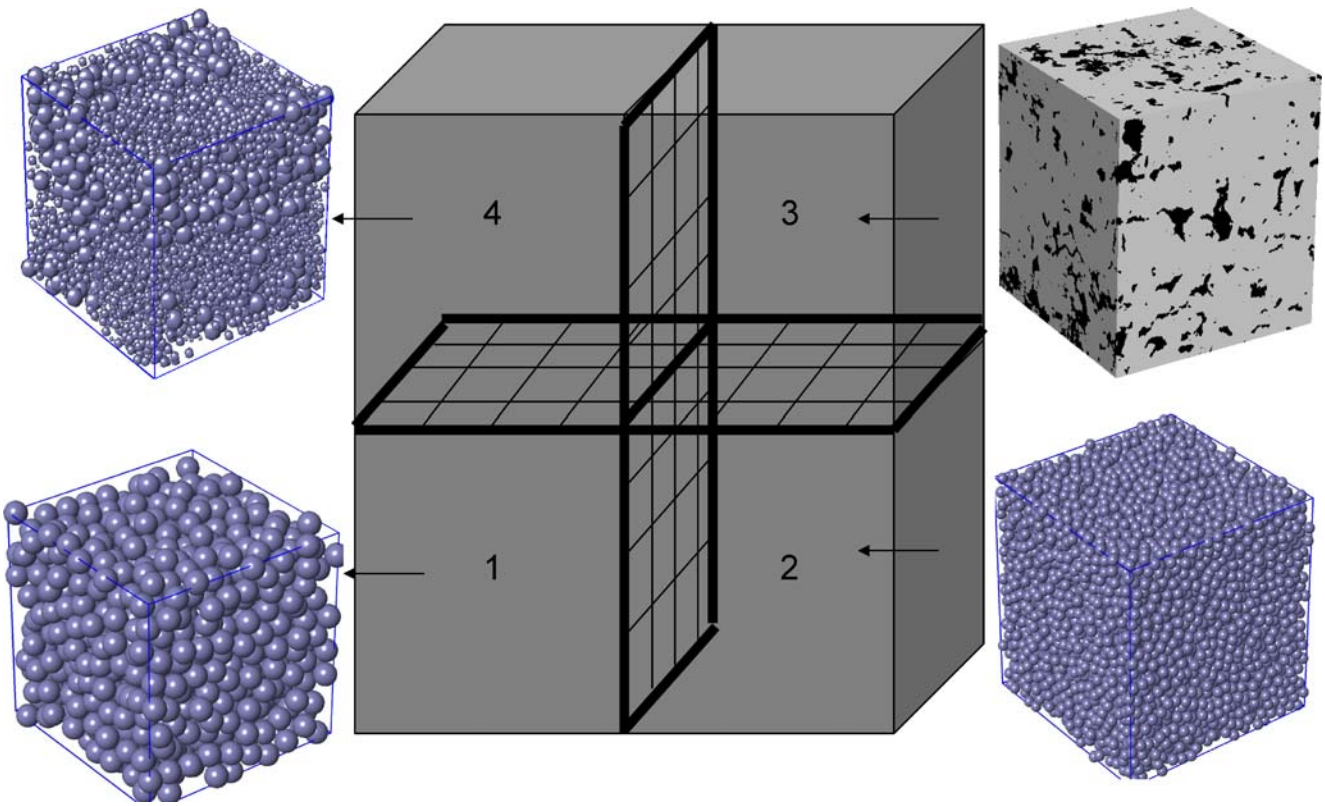

Fig. 7 Schematic of four different pore-scale models arranged in a 2×2 block pattern that are coupled using mortars

Table 3 Summary of network statistics used in coupling simulations

Network	Type	Grains	Pores	Grain (cm)	Permeability (cm^2)	ϕ	Dimensions (cm^3)
1	CG[a]	1,000	4,094	0.053	K_{xx}=1.043 E-05 K_{yy}=1.026 E-05 K_{zz}=1.015 E-05	38	1×1×1
2	CG	10,000	41,273	0.025	K_{xx}=2.469 E-06 K_{yy}=2.413 E-06 K_{zz}=2.411 E-06	38	1×1×1
3	SS[b]	2,487	9,463	~0.020	K_{xx}=2.158 E-07 K_{yy}=1.015 E-07 K_{zz}=8.984 E-08	22	1×1×1
4	CG	10,000	32,496	~0.014	K_{xx}=3.203 E-06 K_{yy}=2.985 E-06 K_{zz}=3.056 E-06	36	1×1×1

[a] CG is a network obtained from computer-generated porous medium.
[b] SS is a network obtained from a real sandstone using XMT. The network size has been rescaled to match the size of the other networks.

Figure 8a is a 2D contour plot of pressure for the four-block pore-scale pattern (the 3D data is collapsed into 2D for clarity). The points represent the location of pore centers in the network model and the color scales the pressure in the pores. The white background is the grain space (the figures do not in any way represent the actual porosity and the denser blocks simply have more pores). A few observations can be made from this figure. First, a continuity of pressure is observed along all of the mortar boundaries, enforced in the domain decomposition, iterative coupling scheme. Second, the results show heterogeneity in the pressure field, which would not be observed if continuum models were used. Figure 8b is pressure field for the same four pore-scale models arranged in a different pattern (from Table 2, network #3 is in the lower-left block, network #2 in the lower-right block, network #4 in the upper-right block, and network #1 in the upper-left block).

The total flow through the domain illustrated in Fig. 8a is 2.26×10^{-3} cm^3/s. The results can be compared to a continuum simulation by using the upscaled permeabilities for each model listed in Table 2. The resulting flowrate is 1.35×10^{-3} cm^3/s, which underestimates the actual flowrate by approximately 40%. In the second simulation (Fig. 8b), the flowrate using the pore-scale models is 1.31×10^{-3} cm^3/s. For this case, the continuum simulation resulted in a 40% overestimation (1.88×10^{-3} cm^3/s). The examples demonstrate the limitations of upscaling macroscopic properties directly by using the pore-scale models as stand-alone tools. Direct upscaling can severely under- or overestimate behavior when coupled to surrounding media.

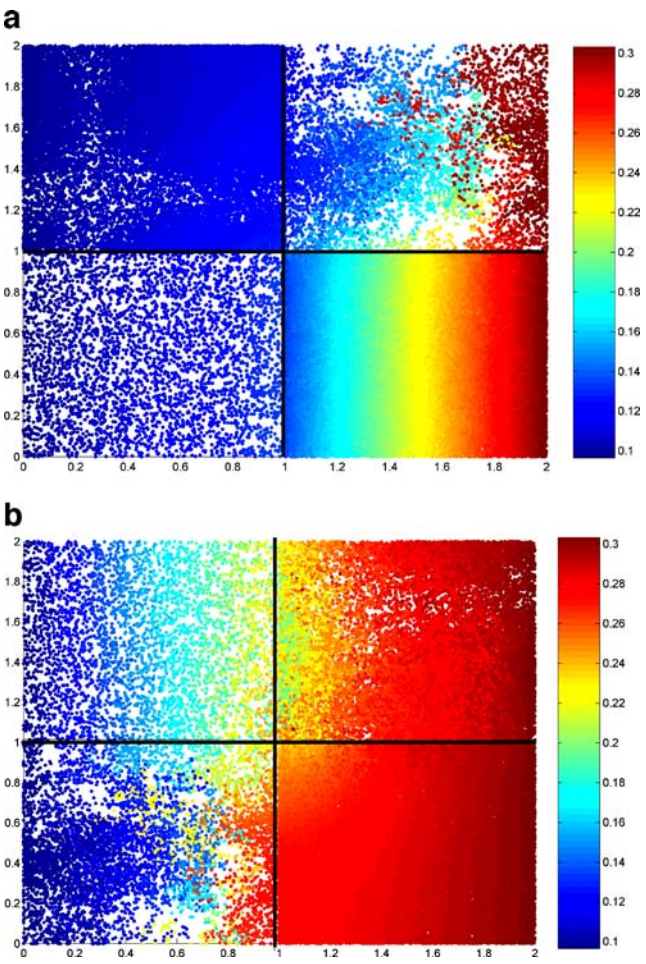

Fig. 8 **a** Contour plot of pressure for results obtained for Fig. 7 problem using 4×4 quadratic mortars for coupling and **b** contour plot for Fig. 7 with alternative block pattern. The data are collapsed into 2D for clarity and the *shaded points* are the pore pressures

4.2 Coupling pore-scale and continuum models

The mortar method used here is not limited to coupling only pore-scale models, it can be easily extended to couple

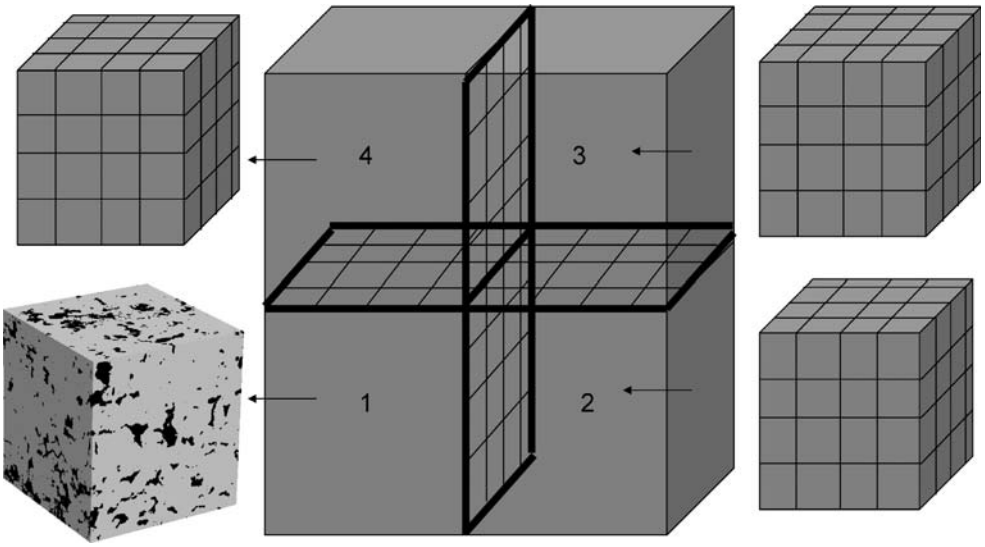

Fig. 9 Schematic of pore-scale model (#3 in Table 2) and three continuum models arranged in a 2×2 block pattern that are coupled using 4×4 quadratic mortars. The continuum blocks have uniform permeability equal to the upscaled value listed in Table 2

pore-scale models to continuum-scale, Darcy models. This application of the mortars is very useful for multiscale modeling, in which the domain is primarily modeled at the continuum scale, but specific regions are modeled at the pore-scale to capture important fundamental behavior.

Figure 9 is a pore-scale network model (#3 in Table 2) coupled to surrounding continuum models. The continuum models are modeled using a 4×4×4 finite difference grid in each block and utilizing Darcy's law. All three blocks are given a uniform permeability, equal to the upscaled values for network model #3 shown in Table 2. A 1D pressure gradient is imposed from right to left for this "simple" problem. The four blocks are coupled using 4×4 quadratic mortars at the interfaces to ensure continuity of pressures and fluxes. It should be noted that the axis is rotated in this simulation so that the flow is actually in the y direction.

Figure 10 is the contour plot of pressure in the domain for the continuum and pore-scale regions, and it is clear that pressure is continuous at the interfaces. If the entire domain had been modeled at the continuum scale (with the permeability also being uniform in the current pore-scale region), then the solution would have been trivial. The pressure would increase linearly from left to right and the streamlines would be straight. In the simulation here, the heterogeneity in the pore-scale region results in a more complicated solution, not only in the pore-scale region but in the continuum region as well, where the permeability is uniform. In Fig. 10, it can be seen that velocity has a vertical component even in the continuum region as a result of the nonuniform boundary conditions obtained through coupling to the pore-scale region.

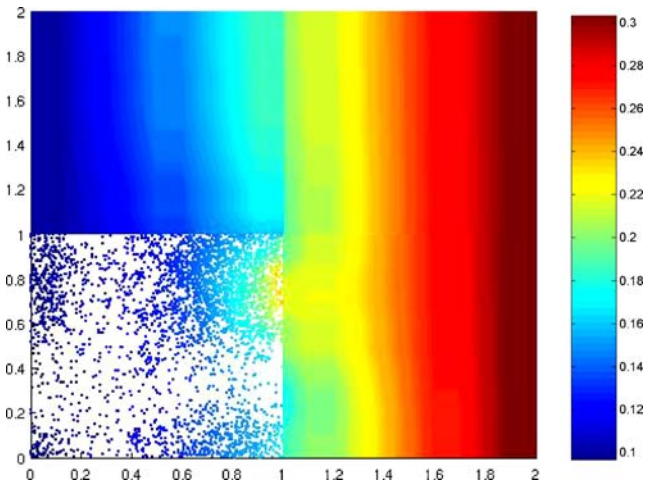

Fig. 10 Contour plot of pressure for pore-scale model coupled to three continuum blocks

The total flow through the domain is 7.90×10^{-5} cm^3, which is about 15% higher than the flowrate (6.76×10^{-5} cm^3/s) obtained from utilizing Darcy's law and the uniform permeability of $K_{yy}=1.015\times10^{-7}$ cm^2. Moreover, the flow exiting the pore-scale region (block 1 in Fig. 9) is 50% higher than the continuum block (#4) directly above it. Although the average, upscaled permeability in the pore-scale region is the same as the other blocks, the natural heterogeneity allows for preferential pathways for flow, and the model acts as a "sink" for fluid to enter from the surrounding blocks. The pressure field in Fig. 10 shows the contour lines bend to allow for flow to enter the pore-scale region. This is another demonstration of the limitations of simple upscaling without imposing realistic boundary conditions on the network model.

5 Conclusions

Although pore-scale models have been used recently as an effective tool for obtaining predictive flow and transport behavior, simple, artificial boundary conditions are usually

implemented. Actual boundary conditions are dependent on the heterogeneity in the pore-scale model itself as well as the surrounding media; they are important because they may affect the qualitative and quantitative results. Here, a method has been developed to couple pore-scale network models to other adjacent pore-scale or continuum-scale models using 2D finite-element mortar spaces at the boundary interfaces. The mortars ensure a pressure boundary condition such that fluxes match weakly at that boundary. The method has been verified by coupling a network model to its exact replica. It is shown both qualitatively and quantitatively that a good approximation is obtained using mortars and that improved accuracy is obtained by implementing a finer mortar discretization and using higher-order basis functions (i.e., linear and quadratic). Quantitative results suggest that coarse meshes and simple basis functions may be suitable for certain problems and the additional computational effort may not be worth the additional accuracy. One important finding of this work is that a decrease in accuracy at the pore-scale can be observed if the mortar mesh is too fine. This can occur because the mortars are intended to match fluxes in an average sense, integrated over an elemental area. If the mesh size is chosen small enough then certain elements will have too few pores and artificial heterogeneity is observed.

Mortars are used to couple four different pore-scale models in a 2×2 block pattern. The pore-scale models have very different pore structures and permeability; the mortars allow for continuity of both pressure and flux at the boundaries. The heterogeneous flow patterns are a result of the heterogeneity in the porous medium as well as the realistic and detailed boundary conditions imposed at the boundary interfaces. Mortars are also used to couple a pore-scale model to surrounding continuum/Darcy models. In the simulation performed here, the network acts as a sink and draws fluid from the surrounding blocks despite having the same average, upscaled permeability as the continuum blocks. This is a result of the heterogeneity and preferential flow pathways in the pore-scale model. These results suggest that simple upscaling from the pore to continuum scales may not be sufficient.

The ability to efficiently couple pore-scale models to other media and to impose realistic boundary conditions has many important implications, and the methodology developed here can be extended to a number of applications. Certain flow and transport phenomena may strongly depend on behavior that occurs upstream. For example, multiphase processes are dynamic; relative permeability and capillary pressure curves may depend on how the phases enter the porous medium. Imposing realistic boundary conditions can result in better upscaled values for substitution in continuum simulators. Another application of this work would involve models that utilize a continuum approach but include select regions that model flow and transport at the pore scale. For example, in reservoir simulation, pore-scale models could be used very close to the well-bore where acidization, particle filtration, non-Darcy flow, etc., are common. The pore-scale region would then be coupled via mortars to the continuum region of the model. Future work will focus on using mortar coupling for these applications and more.

Acknowledgements We would like to thank Karsten Thompson at Louisiana State University for allowing us to use the pore-scale networks presented in this paper in addition to his many suggestions and recommendations. Matthew Balhoff is partially supported by the Institute for Computational Engineering and Sciences postdoctoral fellowship program in addition to grants DOE: DE-FG02-04ER25617 and NSF: CNS-042705. Sunil Thomas and Mary Wheeler are both supported by grants DOE: DE-FG02-04ER25617 and NSF: CNS-042705.

References

1. Adler, P.M., Jacquin, C.G., Thovert, J.: The formation factor of reconstructed porous media. Water Res. **28**(6), 1571–1576 (1992)
2. Al-Raoush, R., Thompson, K.E., Willson, C.S.: Comparison of network generation techniques for unconsolidated porous media. Soil Sci. Soc. Am. J. **67**(6), 1687–1700 (2003)
3. Arbogast, T., Cowsar, L.C., Wheeler, M.F., Yotov, I.: Mixed finite element methods on nonmatching multiblock grids. SIAM J. Numer. Anal. **37**(4), 1295–1315 (2000)
4. Arbogast, T., Pencheva, G., Wheeler, M.F., Yotov, I.: A multiscale mortar mixed finite element method. SIAM Multiscale J. **6**(1):319–346 (2007)
5. Balhoff, M.T., Thompson, K.E.: Modeling the steady flow of yield stress fluids in packed beds. AIChE J. **50**(12), 3034–3048 (2004)
6. Balhoff, M.T., Thompson, K.E.: A macroscopic model for shear-thinning flow in packed beds based on network modeling. Chem. Eng. Sci. **61**(2), 698–719 (2006)
7. Balhoff, M.T., Thompson, K.E, Hjortsø, M.: Coupling pore networks to continuum models. Comput. Geosci. **33**(3), 393–410 (2007)
8. Bakke, S., Oren, P.E.: 3-D pore-scale modelling of sandstones and flow simulations in the pore networks. SPE J. **2**(2), 136–149 (1997)
9. Broughton, J.Q., Abraham, F.F., Bernstein, N., Kaxiras, E.: Concurrent coupling of length scales: methodology and application. Phys. Rev. **13**(60), 2391–2403 (1999)
10. Bryant, S.L., Mellor, D.W., Cade, C.A.: Physically representative network models of transport in porous media. AIChE J. **39**, 387–396 (1993)
11. Gani, M.R., Bhattacharya, J.P.: Bed-scale facies architecture of an ancient delta lobe deposit of the Wall Creek Member, Central Wyoming, U.S.A. AAPG Annual Convention, Official Program. 12, A59, Salt Lake City (2003)
12. Kim, M., Park, E., Thomas, S.G., Wheeler, M.F.: A multiscale mortar mixed finite element method for slightly compressible flows in porous media. J KMS (2007, in press)

13. Klein, P.A., Zimmerman, J.A.: Coupled atomistic-continuum simulations using arbitrary overlapping domains. J. Comput. Phys. **213**, 86–116 (2006)
14. Kohloff, S., Gumbsch, P., Fischmeister, H.F.: Crack propagation in BCC crystals studied with a combined finite-element and atomistic model. Philos. Mag. A. **64**, 851–878 (1991)
15. Liang, Z., Ioannidis, A., Chatzis, I.: Permeability and electrical conductivity of porous media from 3D replicas of the microstructure. Chem. Eng. Sci. **55**, 5247–5262 (2000)
16. Lindquist, W.B., Lee, S., Coker, D.A., Jones, K.W., Spanne, P.: Medial axis analysis of void structure in three-dimensional tomographic images of porous media. J. Geophys. Res. **101**(B4), 8297–8310 (1996)
17. Lindquist, W.B., Venkatarangan, A., Dunsmuir, J., Wong, T.: Pore and throat size distributions measured from synchrotron X-ray tomographic images of Fontainebleau sandstones. J. Geophys. Res. **105**(B9), 21509–21528 (2000)
18. Lopez, X., Valvatne, P.H., Blunt, M.J.: Predictive network modeling of single-phase non-Newtonian flow in porous media. J. Colloid Interface Sci. **264**, 256–265 (2003)
19. Nedelec, J.C.: Mixed finite elements in R^3. Numer. Math. **35**, 315–341 (1980)
20. Peszynska, M., Wheeler, M., Yotov, I.: Mortar upscaling for multiphase flow in porous media. Comput. Geosci. **6**(1), 73–100 (2002)
21. Rudd, R.E., Broughton, J.Q.: Concurrent coupling of length scales in solid state systems. Phys. Status Solidi **217**, 251–291 (2000)
22. Sok, R.M., Knackstedt, M.A., Sheppard, A.P., Pinczewski, W.V., Lindquist, W.B., Venkatarangan, A., Paterson, L.: Direct and stochastic generation of network models from tomographic images. Effect of topology on residual saturations. Transp. Porous Media **46**(2–3), 345–371 (2002)
23. Thompson, K.E., Willson, C.S., White, C.D., Nyman, S., Bhattacharya, J., Reed, A.H.: Application of a new grain-based reconstruction algorithm to microtomography images for quantitative characterization and flow modeling. SPE Annual Technical Conference and Exhibition, 9–12 October, Dallas (2005)
24. Wagner, G.J., Liu, W.K.: Coupling of atomistic and continuum simulations using a bridging scale decomposition. J. Comput. Phys. **190**, 249–274 (2003)
25. Wheeler, M.F., Arbogast, T., Bryant, S., Eaton. J., Lu, Q., Peszynska, M., Yotov, I. A.: Parallel multiblock/multidomain aproach for reservoir simulation. 1999 Symposium on Reservoir Simulation, SPE 51884, Houston (1999)
26. Willson, C.S., Al-Raoush, R.I.: Extraction of physically realistic pore network properties from three-dimensional synchrotron X-ray microtomography images of unconsolidated porous media systems. J. Hydrol. **300**(1), 44–64 (2005)
27. Zhodi, T., Wriggers, P.: A domain decomposition method for bodies with heterogeneous microstructure based on material regularization. J. Solids Struct. **36**, 2507–2525 (1999)